Optimal Simultaneous Allocation of Electric Vehicle Charging Stations and Capacitors in Radial Distribution Network Considering Reliability

B. Vinod Kumar, *Member*, *IEEE* and Aneesa Farhan M A, *Member*, *IEEE*

***Abstract*—The popularity of electric vehicles (EVs) has sparked a greater awareness of carbon emissions and climate impact. Urban mobility expansion and EV adoption have led to an increased infrastructure for electric vehicle charging stations (EVCSs), impacting radial distribution networks (RDNs). To reduce the impact of voltage drop, the increased power loss (PL), lower system interruption costs, and proper allocation and positioning of the EVCSs and capacitors are necessary. This paper focuses on the allocation of EVCS and capacitor installations in RDN by maximizing net present value (NPV), considering the reduction in energy losses and interruption costs. As a part of the analysis considering reliability, several compensation coefficients are used to evaluate failure rates and pinpoint those that will improve NPV. To locate the best nodes for EVCSs and capacitors, the hybrid of grey wolf optimization (GWO) and particle swarm optimization (PSO) (HGWO_PSO) and the hybrid of PSO and Cuckoo search (CS) (HPSO_CS) algorithms are proposed, forming a combination of GWO, PSO, and CS optimizations. The impact of EVCSs on NPV is also investigated in this paper. The effectiveness of the proposed optimization algorithms is validated on an IEEE 33-bus RDN.**

***Index Terms*—Electric vehicle charging station, optimization, radial distribution network, vehicle-to-grid, loss reduction, reliability.**

I. Introduction

THE dependence of transportation sector on fossil fuels leads to hazardous CO_2 emissions that impact the environment. For greener communities, moving to electric vehicle (EV) will expand public transportation, and encourage active travel [1]. EVs have many benefits, including economic advantages, exceptional performance, and a positive environmental effect by reducing the harmful pollutants caused by transportation. By 2030, India's National Electric Mobility Mission Plan (NEMMP) 2020 and Faster Adoption and Manufacturing of Electric Vehicles (FAME) 2015 programme target EV adoption. Researchers are looking at where to allocate EV charging stations (EVCSs) due to the rise of EVs. However, there are obstacles to deploy EVs widely, e.g., the demand for charging stations and the determination of charging time. We require effective charging stations to operate effectively [2]. Robust grids and less power loss (PL) are required to manage EVs effectively [3]. Grid-to-vehicle (G2V) energy transfer is facilitated by smart grids [4]. The number of charging station installations increases with the adoption of EV [5]. Charging stations have improved voltage profiles with capacitors, increasing their efficiency when allocated properly [6], [7].

Numerous important advancements have been made in power system optimization and improvement over time. Early efforts such as [8] emphasized on the optimization to save costs, improve overall benefits, and reduce losses in power systems. Later research work dug into other facets of power system management. Notably, [9] carried out a thorough investigation of reliability analysis, providing ways to improve the power system flexibility. Since the early 2000s, there has been interest in capacitor placement, which is a key strategy for voltage regulation. Reference [10] presented the idea of employing particle swarm optimization (PSO) to optimize voltage profiles, allocate capacitors strategically, and reduce PLs. After ten years, in [11], a two-phase strategy was successfully used to allocate EVCS in line with the increasing demand for effective EV infrastructure. Reference [12] focused on the infrastructure needed for EV charging. Additionally, [13] clarified how short-range EV charging affects PLs, highlighting the demand for optimized solutions.

Modern optimization methods have been incorporated into power system management in recent years. Reference [14] suggested a hybrid strategy combining weight improved particle swarm optimization (WIPSO) and gravitational search algorithm (GSA), called WIPSO-GSA, for capacitor and distributed generation (DG) unit optimization. This was a huge step in the direction of more thorough optimization techniques. In [15], attempts were made to boost power system stability by enhancing the reliability of networks utilizing mixed-integer nonlinear programming and AC optimization. In [16], a quantum-inspired capacitor design algorithm was presented as the result of the convergence of quantum algorithms and power system optimization. The development allowed more effective capacitor placement techniques by merging classical optimization with fundamental concepts. Based on this, [17] integrated PSO and grey wolf optimization (GWO) with the hybrid of GWO and PSO (HGWO_PSO), presenting improved optimization results. Recent

Manuscript received: September 18, 2023; revised: November 21, 2023; accepted: January 24, 2024. Date of CrossCheck: January 24, 2024. Date of online publication: April 18, 2024.

B. V. Kumar and A. F. M A (corresponding author) are with the Department of Electrical and Electronic Engineering, National Institute of Technology Tiruchirappalli, Tamilnadu, India (e-mail: vnu056@gmail.com; aneesafma@gmail.com).

DOI: 10.35833/MPCE.2023.000674

developments also address the complex combination between DG and EVCS. Considering their combined influence on the power system, [18] used the HGWO_PSO to optimize the choices of EVCS and DG units. Multi-objective framework was also established in [19] to optimize EVCS comprehensively while considering various objectives.

To economically arrange capacitors while accounting for practical factors, [20] proposed a method that combined load flow (LF) analysis, Shannon's entropy, and PSO. Meanwhile, [21] demonstrated the effectiveness of mixed-integer linear programming (MILP) in optimizing capacitor deployment by streamlining the optimization procedures. As time progresses, state-of-the-art research work continues to advance power system management techniques. Notably, [22] showcased a hybrid technology of Eurasian oystercatcher optimizer (EOO) and quantum neural network (QNN), called EOO-QNN, which improved voltage, PL, and reliability, underscoring ongoing efforts to enhance power system optimization and reliability. In parallel, recent research works have delved into the impact of intensive EV charging on power distribution systems and transformer longevity [23]. Reference [24] explored concerns related to overloading and undervoltage due to the increasing adoption of EVs, employing software tools such as DRIVE and HotSpotter. To effectively manage power systems while integrating EVs, energy storage, and renewable sources, an MILP model was introduced in [25], which led to cost reduction and reduced carbon emissions. Additionally, [26] investigated using metaheuristic algorithms to optimize battery energy storage systems, thereby improving performance and cost-effectiveness in radial distribution network (RDN) with photovoltaics (PVs) and EVs. To reduce uncertainty and user discomfort by 17%, [27] presented an EV charging scheduling method based on the alternating direction method of multipliers (ADMM) algorithm. Furthermore, [28] examined the capacity of RDN to support EV charging within the context of demand response. These references addressed the complex challenge of integrating EVs into power distribution systems and highlighted the evolving strategies and technologies in power system design and management.

This paper focuses on optimal simultaneous allocation of EVCSs and capacitors in RDN considering reliability, helping to improve voltage, reduce PL, and increase profit in RDN. Consequently, the primary contributions of this paper are as follows.

1) The backward-forward sweep (BFS) algorithm is used to conduct LF studies in IEEE 33-bus RDN for the base case after connecting EVCSs and capacitors.

2) An objective function based on the benefit of energy loss reduction, expected interruption cost (EIC), and interruption cost is proposed for this optimal simultaneous allocation problem. Accordingly, after connecting EVCSs and capacitors, new failure rates are updated, and EIC is computed.

3) Multiple cases of various capacitance and EVCS operation conditions are considered to find out the optimal number of nodes, size of capacitors, and EVCSs in the RDN.

4) The optimization algorithms, i.e., HGWO_PSO and the hybrid of PSO and Cuckoo search (HPSO_CS), are proposed as a solution to the optimization problem.

5) The proposed optimization algorithms are validated in IEEE 33-bus RDN with EVCSs and capacitors.

6) Finally, a comparison of the proposed optimization algorithms for the simultaneous allocation of EVCSs and capacitors in the RDN is carried out.

The rest of the paper is structured as follows. Section II presents the mathematical model formulation. In Section III, the solution techniques based on optimization are discussed. Results and discussion are presented in Section IV. Section V concludes this paper.

II. Mathematical Model Formulation

A. Benefit Due to PL Reduction

PL computation is crucial in any RDN, as it impacts revenue and helps the planning operators.

1) Computation of Base Case PL

The BFS algorithm estimates the voltage and current in the RDN. Accordingly, the current and the network parameters (R_i, X_i) are used to compute the losses in the RDN including active power loss (APL) and reactive power loss (RPL). The APL impacts the revenue in RDN. Equation (1) gives the APL computed considering base case conduction where no EVCS and capacitor are present [29].

$$P_{loss,i} = \sum_{i=1}^{N_{br}} I_i^2 R_i \tag{1}$$

where $P_{loss,i}$ is the total base case APL; R_i is the ohmic resistance of the i^{th} branch; N_{br} is the total number of branches; and I_i is the current flowing through the i^{th} branch.

2) Computation of PL Compensation

To compute PL compensation, both EVCSs and capacitors are considered. EVCS can behave as a load during charging, i.e., in G2V mode, and it can be operated in vehicle-to-grid (V2G) mode to reduce grid stress by discharging during peak hours. Here, the charging station load is modeled using the active power (AP) at unity power factor (UPF). The total load in the RDN P_{load} [30] comprises both grid power load and charging station load.

$$\begin{cases} P_{load} = \sum_{bs=1}^{N_{bs}} (P_{bs}^{al} + \gamma P_{bs}^{CS}) \\ \gamma = 1 \quad \text{G2V mode} \\ \gamma = -1 \quad \text{V2G mode} \end{cases} \tag{2}$$

where P_{bs}^{al} is the available load of the system; P_{bs}^{CS} is the charging station load connected to buses; and N_{bs} is the total number of buses. The total reactive power (RP) load of the system is the sum of the available RP load Q_{bs}^{al} of the system and the RP injected by the capacitor load Q_{bs}^{C} of the system. Hence, the total RP of the system is given by:

$$Q_{load} = \sum_{bs=1}^{N_{bs}} (Q_{bs}^{al} - Q_{bs}^{C}) \tag{3}$$

Thus, the net benefit due to PL reduction PE_{LRD} is given by:

$$PE_{LRD} = E_{cp}(P_{loss,base} - P_{loss,comp})T \tag{4}$$

where E_{cp} is the energy price; T is the time period for the year in hours ($T = 8760$); $P_{loss,base}$ is the computed PL for the base case; and $P_{loss,comp}$ is the compensated PL after installing

EVCSs and capacitors, using the BFS algorithm.

B. Evaluation of EVCS and Capacitor Cost

1) Installation Cost of EVCSs and Capacitors

The total installation cost of EVCSs and capacitors consists of the location costs, equipment cost, monitoring cost, and miscellaneous costs. The equation for the installation cost of EVCSs is:

$$C_{ins}^{CS}=\varphi\left(C_{insl}^{CS}\cdot CS_n+C_{Pcost}^{CS}\sum_{i=1}^{CS_n}P_{CS,inj}(i)\right) \tag{5}$$

where CS_n is the standard number of EVCSs; C_{Pcost}^{CS} is the purchase cost of EVCSs; and $P_{CS,inj}$ is the EVCS power injected to the network.

The installation cost of capacitor C_{ins}^{C} is given by:

$$C_{ins}^{C}=\varphi\left(C_{insl}^{C}C_n+C_{Pcost}^{C}\sum_{i=1}^{C_n}Q_{C,inj}(i)\right) \tag{6}$$

where C_n is the standard number of capacitors; C_{Pcost}^{C} is the purchase cost of capacitor; $Q_{C,inj}$ is the RP injected to the network; and φ is a depreciation factor given by:

$$\varphi=\frac{ir\cdot(1+ir)^{L_{sp}}}{(1+ir)^{L_{sp}}-1} \tag{7}$$

where ir is the discount rate; and L_{sp} is the life span of project.

2) Operation Costs of EVCSs and Capacitors

The operation costs of EVCSs and capacitors include fuel costs and yearly inspections for electrical and mechanical systems, which are calculated as:

$$C_{opr}=C_{opr}^{C}C_n+C_{opr}^{CS}\cdot CS_n \tag{8}$$

where C_{opr} is the operation cost in location per year of EVCSs C_{opr}^{CS} and capacitor C_{opr}^{C}.

C. Benefit Due to Interruption Cost Reduction

1) Reliability Evaluation

Although RDN provides consumers with one-way electricity, this one-way electricity is less efficient and resilient due to localized outages. Busbars, disconnects, lines, and cables are just some of the system components, which should be present to remain effective system operation. The system performance and characteristics of outages are directly assessed using the reliability metrics U_{RS}, λ_{RS}, and r_{RS} as:

$$\begin{cases}U_{RS}=\sum_{j=1}^{N_{FS}}r_j\lambda_j\\ \lambda_{RS}=\sum_{j=1}^{N_{FS}}\lambda_j\end{cases} \tag{9}$$

$$r_{RS}=\frac{U_{RS}}{\lambda_{RS}}=\frac{\sum_{j=1}^{N_{FS}}r_j\lambda_j}{\sum_{j=1}^{N_{FS}}\lambda_j} \tag{10}$$

where r_j and λ_j are the average outage length and failure rate, respectively; $r_j\lambda_j$ is the yearly outage of the j^{th} feeder section (FS); and N_{FS} is the number of FSs in RDNs.

The following assumptions are considered when assessing EIC for addressing concerns on optimal installation of EVCSs and capacitors.

1) The FS with the highest impedance has a failure rate of 50%, and the FS with the lowest impedance has a failure rate of 10% annually [31]. The failure rates of the other FSs are determined linearly based on these two impedance values as shown in (11). The j^{th} FS has a Z_j impedance and a λ_j failure rate. The maximum and minimum impedance values are $Z_{\max}$ and $Z_{\min}$, respectively. Since the failure rate and line length are inversely proportional, longer lines have higher failure rates.

$$\lambda_j=\frac{10\%+(50\%-10\%)}{\frac{Z_{\max}-Z_{\min}}{Z_j-Z_{\min}}} \tag{11}$$

2) It is assumed that the transient faults of overhead distribution line are handled with electronic sectionalizes and primary breakers. Hence, fixing each FS takes about 0.5 hour [14], [31], while the repair time is 8 hours [31], [32].

When shunt capacitors of varying sizes are optimally placed in the distribution system, RP compensation is provided, which is in the reactive current component of the system. Similarly, when EVCS is integrated into the RDN, it acts as active power load, which are also reflected in the active current component of the system. Thus, the installation of EVCSs and capacitors in the RDN impacts active and reactive current components. In the RDN, the compensation coefficient refers to the ratio of the new current I_j^{new} (obtained after the allocation of EVCSs and capacitors) and the base current I_j^{base} (before the allocation of EVCSs and capacitors). This compensation coefficient can be more or less than 1, based on whether the new current is greater or smaller than the base current.

$$\Psi_j=\left|\frac{I_j^{new}}{I_j^{base}}\right| \tag{12}$$

where Ψ_j is the symbol indicating the compensation coefficient of the branch for the j^{th} FS, e.g., a high compensation coefficient after a failure will indicate an increase in current, which could help choose defensive devices to keep the system secure. Here, three compensation coefficients are considered and denoted as Ψ_j^{Ai} ,Ψ_j^{Ri}, and Ψ_j^{ARi}. Ψ_j^{Ai} is used to represent the active current compensation applicable when only EVCS is considered, Ψ_j^{Ri} represents the reactive current compensation applicable when only the capacitor is considered, and Ψ_j^{ARi} represents the reactive current compensation applicable when both EVCS and capacitor are considered. The equations representing the compensation coefficient of these three cases to compute the failure rate are as follows.

$$\begin{cases}\Psi_j^{Ai}=\left|\frac{I_j^{Ai,new}}{I_j^{Ai,base}}\right|\\ \Psi_j^{Ri}=\left|\frac{I_j^{Ri,new}}{I_j^{Ri,base}}\right|\end{cases} \tag{13}$$

$$\Psi_j^{ARi}=\left|\frac{I_j^{new}}{I_j^{base}}\right|=\frac{\sqrt{(I_j^{Ai,new})^2+(I_j^{Ri,new})^2}}{\sqrt{(I_j^{Ai,base})^2+(I_j^{Ri,base})^2}} \tag{14}$$

where $I_j^{Ai,new}$ and $I_j^{Ri,new}$ are the currents after the allocation of the EVCSs and capacitors, respectively; $I_j^{Ai,base}$ and $I_j^{Ri,base}$ are the initial active and reactive currents, respectively.

The absolute value of Ψ_j is utilized for all the above cases. To eliminate the current direction due to failure, Ψ_j^{ARi} considers both I_j^{Ai} and I_j^{Ri}, whereas Ψ_j^{Ai} and Ψ_j^{Ri} consider only I_j^{Ai} and I_j^{Ri}, respectively. After optimizing the EVCSs and capacitors, the failure rate of the j^{th} FS, λ_j^{base}, lowers to 80% [31], [33]. The allocation of EVCSs and capacitors linearly impacts the failure rate. The new failure rate λ_j^{new} is computed as:

$$\lambda_j^{new} = \Psi_j(\lambda_j^{base} - \lambda_j^{comp}) + \lambda_j^{base} \tag{15}$$

where λ_j^{base} is the failure rate before the allocation of EVCS and capacitor; and λ_j^{comp} is the failure rate after the allocation of EVCS and capacitor.

2) Evaluation of EIC

The EIC [31]-[33] helps compute the customer reliability levels, thereby boosting maintenance by providing solutions. EIC is calculated for the j^{th} FS as:

$$EIC_j = \sum_{j}^{N_{bs}} L_{a,j} C_j \lambda_j \tag{16}$$

$$\lambda_j = \begin{cases} \lambda_j^{base} & \text{without compensated} \\ \lambda_j^{new} & \text{fully compensated} \end{cases} \tag{17}$$

where $L_{a,j}$ is the average load connected to the load point; and C_j is the interruption cost for the bus for the j^{th} FS. C_j is calculated using the composite customer damage function (CCDF) and $L_{a,j}$, and captured by CCDF based on the length of interruption, as shown in Table I [34]. Also, the interruption cost varies according to the location of the fault event and how long it takes to resolve. When the EVCS and capacitor are not present, $\lambda_j = \lambda_j^{base}$; but when they are present, $\lambda_j = \lambda_j^{new}$.

TABLE I
AVERAGE INTERRUPTION COST OF COMMERCIAL CUSTOMERS

Duration category (min)	Interruption cost ($/kW)
Momentary (less than 0 s)	0.22
3	0.25
20	0.71
60	2.02
120	4.09
240	8.34
1440	27.71

3) Benefit Due to EIC Reduction

The lowered EIC benefits from capacitor installation and post-optimal EVCS are calculated in this paper. The benefit due to interruption cost reduction in EIC, ΔP_{EIC}, is calculated by:

$$\Delta P_{EIC} = E_{cp}(EIC_{base} - EIC_{comp}) \tag{18}$$

where EIC_{base} is the EIC without EVCS and capacitor; and EIC_{comp} is the EIC with EVCS and capacitor.

D. Objective Function and Constraints

1) Economic Evaluation

The financial viability of a capacitor installation must be evaluated by comparing expected earnings and investment expenditures throughout the project, including advantages realized and investments made to reduce failure rates, and maintenance time and costs. For the investments to be profitable, the net present value (NPV) must be positive compared with the costs, as shown in (19). A high NPV promotes acceptance because it shows an increase in utility, while a low NPV discourages acceptance since it shows a likely decline in utility. NPV subtracts the initial investment cost (IC) from the benefit obtained from PL reduction and interruption cost reduction, considering discounted yearly cash flows.

$$NPV = (PE_{LRD} + \Delta P_{EIC}) - IC \tag{19}$$

$$IC = C_{ins} + C_{opr} \tag{20}$$

$$C_{ins} = C_{ins}^{C} + C_{ins}^{CS} \tag{21}$$

2) Equality Constraints

The grid supply P^{supply} should equal the sum of APL and the overall load of the system and EVCS loads.

$$P^{supply} = \sum_{j=1}^{N_{br}} P_{loss}^{j}(m,n) + \sum_{b=1}^{N_{bs}} P_b^{al} + \sum_{b=1}^{N_{bs}} P_b^{CS} \tag{22}$$

where $P_{loss}^{j}(m,n)$ is the APL in line j between buses m and n.

The RP supplied from the grid and capacitor should be equal to the total RP load of the system.

$$Q^{supply} + \sum_{b=1}^{N_{bs}} Q_C(b) = \sum_{j=1}^{N_{br}} Q_{loss}^{j}(m,n) + \sum_{b=1}^{N_{bs}} Q_b^{al} + \sum_{b=1}^{N_{bs}} Q_b^{CS} \tag{23}$$

where Q^{supply} is the total RP supplied by the grid; and Q_C is the RP provided by all capacitors installed at the buses.

3) Inequality Constraints

1) Limit on bus voltage and current

$$\begin{cases} V_b^{\min} \le V_b \le V_b^{\max} \\ 0 \le I_r \le I_r^{\max} \end{cases} \tag{24}$$

where $V_b^{\min}$ and $V_b^{\max}$ are the minimum and maximum allowable voltage at bus b; I_r is the current flowing through line or branch r, respectively; and $I_r^{\max}$ is the maximum allowable current in line or branch r.

2) Limit on size of capacitor

$$Q_C^{\min} \le \sum_{b=1}^{N_{bs}} Q_{C,nbs} \le Q_C^{\max} \tag{25}$$

where $Q_C^{\min}$ and $Q_C^{\max}$ are the minimum and maximum total RP capacities that can be provided by capacitors, respectively; and $Q_{C,nbs}$ is the RP provided by capacitors across all buses.

3) Limit on size of EVCS

$$P_{CS}^{\min} \le \sum_{b=1}^{N_{bs}} P_{CS,b} \le P_{CS}^{\max} \tag{26}$$

where $P_{CS}^{\min}$ and $P_{CS}^{\max}$ are the minimum and maximum total active power capacities that can be handled by all EVCSs in the system; and $P_{CS,b}$ is the active power demand of EVCS across all locations.

4) Limit on RP compensation provided by capacitor

$$\sum_{n=1}^{c_n} Q_C(n) \leq \sum_{b=1}^{N_{bs}} Q_b^{ad} \tag{27}$$

where $\sum_{n=1}^{c_n} Q_C(n)$ is the total RP compensation provided by all capacitors; and $\sum_{b=1}^{N_{bs}} Q_b^{ad}$ is the total reactive power demand in the system that needs to be compensated.

III. Solution Techniques Based on Optimization

In the computation of the objective function, three key components are evaluated: the benefit of reduction in energy loss cost, the benefit of EIC reduction, and the IC. The APL becomes an important factor in evaluating energy loss reduction. The PL is determined using (1), and the failure rate becomes a pivotal factor in evaluating the EIC reduction. The failure rate is determined by a compensation coefficient computed using the branch current, and the operation and installation costs are used to evaluate the IC. The unknown decision variables in this formulation of the objective function as a nonlinear mixed-integer problem include capacitor position, capacitor rating, and system failure rate. Classical methods for solving this optimization are computationally complex, and hence, metaheuristic algorithms are proposed in the literature to ensure near-optimal solutions. Metaheuristic algorithms have gained popularity due to their simplicity, flexibility, and problem-solving efficiency in optimizing the integration of various electrical units like DG, EV, and power electronics devices, e. g., capacitor, static synchronous compensator, voltage regulators, for better power delivery and compensation [35], [36].

In this paper, HGWO_PSO and HPSO_CS are proposed. These hybrid algorithms offer significant advantages such as rapid convergence, the ability to maintain equilibrium in complex systems, and an increase in overall problem-solving effectiveness, efficiently tackling the complex problems associated with electrical unit integration within RDN.

A. HPSO_CS

The social behavior of fish or bird inspires the PSO. On the one hand, the PSO includes benefits like simple operation, quick searching, and ease of understanding. On the other hand, PSO gets easily caught in the local optimum while solving a large and complex problem. To make PSO easier to utilize, this problem must be overcome, which is enabled by using CS. The nesting behavior inspires the CS. In CS, the search procedure quickly switches from one location to another due to the outstanding randomness of Levy flight. As a result, the ability of the algorithm to search globally is highly developed. Due to the extreme randomness of the Levy flight, the algorithm begins a blind search process, the convergence speed slows down, and the searching efficiency is substantially reduced close to the optimal solution. Hence, we propose a hybrid algorithm based on PSO and CS, which combines the benefits of both PSO and CS. The PSO will repeatedly improve the population by updating the position and velocity of the particles based on their best position across all the particles. The CS generates new solutions for the population based on the Cuckoo's probabilistic egg-laying and nest-searching processes and determines the fitness of those solutions. The particle is replaced with the lowest performance if CS works better than a PSO. Consequently, the PSO offers an equal amount of global and local search, and CS helps to improve global exploration. Thus, the HPSO_CS [37] helps get better optimization results than the individual optimization algorithm. The pseudo-code and the relevant equation required to define the algorithm are shown in Algorithm 1, where V_i is the velocity of particle i at current time step t; W is the inertic weight; and θ is the scaling factor that adjusts the step size of Levy flight.

Algorithm 1: pseudo-code of HPSO_CS

Input: search agent, parameters of PSO and CS

Output: best fitness function

Initialization: the parameters L_b, U_b, n, $W_{\max}/W_{\min}$, C_1, C_2, r_1, r_2, P_a

Randomly generate the initial position of particles within the limited range X_i

While t is less than the maximum generation or other stop criterion **do**

Call for PSO

Calculate fitness of each particle by objective function $f(X_i)=f_i$

Update the velocity and position of each particle by using

$$V_i(t+1)=WV_i(t)+C_1r_1(P_{best}(t)-X_i(t))+C_2r_2(G_{best}(t)-X_i(t))$$
$$X_i(t+1)=X_i(t)+V_i(t+1)$$

for each particle **do**

Evaluate the fitness of each particle of objective function P_{best_i} and G_{best_i}, and select the best particle of Gbest position based on best fitness value

$$P_{best_i}(t+1)=\begin{cases} X_i(t+1) & f(X_i(t+1))<f(X_i(t)) \\ P_{best_i} & \text{otherwise} \end{cases}$$
$$G_{best_i}(t)=\min\{P_{best_{i1}}(t),P_{best_{i2}}(t),\ldots,P_{best_{iN}}(t)\}$$

end (for loop)

Call for Cuckoo

for each particle **do**

Find a best nest by CS

end (for loop)

A friction P_a of the worst-performing particle is chosen in terms of the fitness function. The chosen particles should be dropped from the search space and replaced with randomly generated ones.

r_1 and r_2 vary with Levy flight, which is different form the HPSO_CS

$$V_i(t+1)=WV_i(t)+[c_1\theta Levy(\beta)(P_{best}(t)-X_i(t))]+[c_2\theta Levy(\beta)(G_{best}(t)-X_i(t))]$$

Record the optimal solution of the current iteration

$t=t+1$ (iteration step increases)

If the termination criterion is not met, go to Step 6

end (while loop)

B. HGWO_PSO

The GWO and PSO are nature-inspired optimization algorithms inspired by the hunting behavior of grey wolves and the social behavior of fish or bird. The main difference between GWO and PSO is how new individuals are formed. In this paper, HGWO_PSO is suggested to achieve the benefits

of both algorithms. When the hybridization operates, the GWO first updates the wolf position, including α, β, and δ wolf solutions. After that, the wolves adjust their position, which depends on the hierarchy of the wolf pack and how close they are to α, β, and δ wolves. Additionally, after each position is adjusted by GWO, each updated position modifies its velocity using the PSO. The previous velocity, the local best position of individual, and the global best position of the population are all considered while updating the velocity, which improves the current solution by utilizing the most up-to-date information. Each wolf or particle in the population maintains a record of the best solution encountered during the optimization process. The best solution found by any individual in the entire population is the shared information, representing the overall best solution among all individuals. HGWO_PSO leads participants toward their fitness solution positions to enable delicate exploitation and improve convergence while optimizing the locations of EVCSs and capacitors toward the best solutions. The pseudo-code [38] of HGWO_PSO is shown in Algorithm 2, where X denotes the current position of the wolf being updated; $\vec{X}_1$, $\vec{X}_2$, and $\vec{X}_3$ denote the intermediary positions calculated using the influence of α, β, and δ, respectively; and $\vec{(\cdot)}$ denotes the vector.

Algorithm 2: pseudo-code of HGWO_PSO

Input: search agents, parameters of GWO and PSO
Output: optimal solution
Initialization: the parameters L_b, U_b, n, $W_{\max}/W_{\min}$, C_1, C_2, r_1, r_2, a, A, and C
Generate initial population randomly within the search space range
Call GWO algorithm
Calculate the fitness value of α, β, and δ

$$\vec{D}_\alpha=|\vec{C}_1\vec{C}_\alpha-\vec{X}|,\ \vec{D}_\beta=|\vec{C}_2\vec{C}_\beta-\vec{X}|,\text{ and }\vec{D}_\delta=|\vec{C}_3\vec{C}_\delta-\vec{X}|$$

Update the position of each wolf of current wolf by using

$$\vec{X}_1=\vec{X}_\alpha-\vec{A}_1(\vec{D}_\alpha),\ \vec{X}_2=\vec{X}_\beta-\vec{A}_2(\vec{D}_\beta),\ \vec{X}_3=\vec{X}_\delta-\vec{A}_3(\vec{D}_\delta)$$

While t is less than the maximum generation or other stop criterion **do**
  for each search agent **do**
    Update the position of current wolf search agent $\vec{X}_{new}$ by using

$$\vec{X}_{t+1}=\frac{\vec{X}_1+\vec{X}_2+\vec{X}_3}{3}$$

  end (for loop)
  Update the best wolf that achieves the best fitness value
  Call PSO algorithm
  for each search agent **do**
    Update the particle velocity and position by using

$$V_i(t+1)=WV_i(t)+C_1r_1(P_{best}(t)-X_i(t))+C_2r_2(G_{best}(t)-X_i(t))$$
$$X_i(t+1)=X_i(t)+V_i(t+1)$$

  end (for loop)
    Compute the fitness function of each particle P_{best} and G_{best}
  for each search agent **do**
    Update a, A, and C, and calculate the fitness value for all wolves
  end (for loop)
  Update the fitness value of α, β, and δ wolf positions
  $t=t+1$ (iteration step increases)
end (while loop)

C. Proposed Optimization Algorithms

The proposed optimization algorithms aim to achieve the optimal simultaneous allocation of EVCSs and capacitors in a RDN while considering reliability. The algorithm follows a series of steps outlined in Fig. 1. The optimization process is conducted under different operation conditions, each represented by a specific case involving EVCSs and capacitors. These cases are defined as follows:

1) Case 1: one capacitor (1C) + two EVCSs.
2) Case 2: two capacitors (2C) + two EVCSs.
3) Case 3: three capacitors (3C) + two EVCSs.
4) Case 4: four capacitors (4C) + two EVCSs.
5) Case 5: five capacitors (5C) + two EVCSs.
6) Case 6: six capacitors (6C) + two EVCSs.

Figure 1 illustrates the flow chart for optimal allocation of EVCS and capacitor using the proposed optimization algorithms. In various optimization algorithms, values for the parameters are considered as follows.

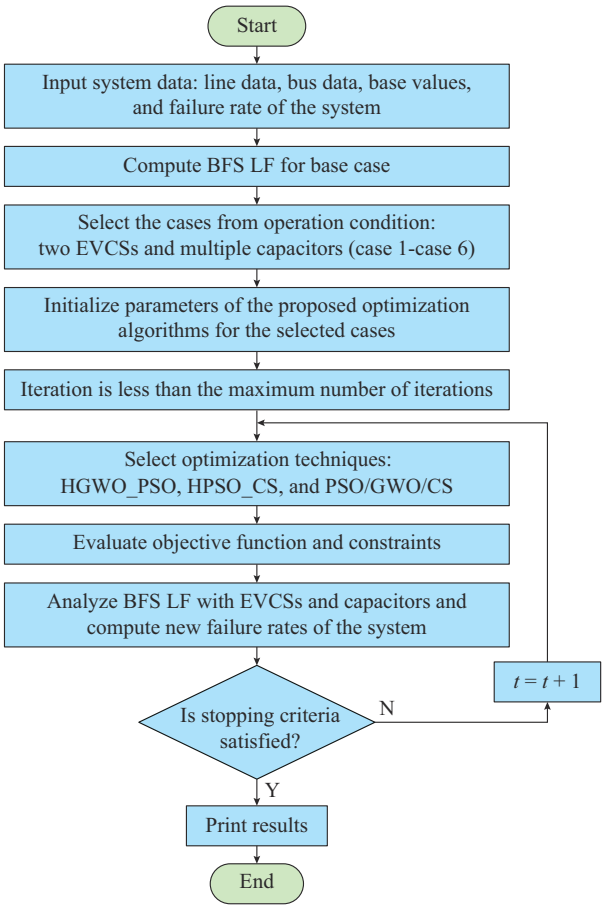

Fig. 1. Flow chart of optimal allocation of EVCSs and capacitors using proposed optimization algorithms.

The maximum iteration is 1000, the search agents are 10-30, the swarm size is 30-50, $W_{\min}$ is 0.4, $W_{\max}$ is 0.9, C_1 is 2.01, C_2 is 2.02, P_a is within [0, 1], $\vec{a}$ is 2 to 0, and r_1 and r_2 are random numbers within [0, 1].

In this paper, five separate scenarios are examined to validate the methodology.

1) Scenario 1: base case, i.e., IEEE 33-bus RDN [39].
2) Scenario 2: EVCS1 integrated with RDN.

3) Scenario 3: both EVCSs (EVCS1 and EVCS2) integrated with RDN.

4) Scenario 4: multiple installations of EVCSs and capacitors with RDN.

5) Scenario 5: impact of V2G mode of EVCSs on the RDN.

IV. Result and Discussion

Although EVs can operate in V2G mode, the initial focus is to consider EVs as EVCS loads. The EVCS in this paper is modeled and used as a constant power load in the RDN. The proposed optimization algorithms are tested using the IEEE 33-bus RDN, schematically shown in Fig. 2, which has 33 nodes and 32 branches with a base voltage and system capacity of 12.66 kV and 100 MVA, respectively. The IEEE 33-bus RDN is a balanced three-phase network with an AP load of 3715 kW and an RP load of 2300 kvar. The constant parameters are shown in Table II [7], [17].

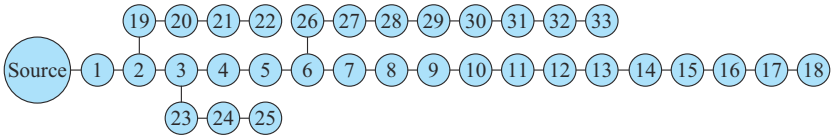

Fig. 2. Structure of IEEE 33-bus RDN.

TABLE II
Constant Parameters

Parameter	Unit	Value
C^{C}_{Pcost}	$/kvar	30
C^{CS}_{Pcost}	$/kW	10
E_{cp}	$/kWh	0.06
T	hour	8760
C^{C}_{insl}	$ per location	1600
C^{CS}_{insl}	$ per location	6500
C^{C}_{opr}	$/year per location	350
C^{CS}_{opr}	$/year per location	8500
ir	%	6
L^{C}_{sp}	year	30
L^{CS}_{sp}	year	15

A. Scenario 1

Initially, for the base case using the BFS algorithm, the APL and RPL obtained for the IEEE 33-bus RDN are 204.7920 kW and 136.9346 kvar, respectively. Figure 3 depicts the base case voltage profile of IEEE 33-bus RDN, showing that bus 18 has the lowest voltage of 0.9162 p.u..

B. Scenarios 2 and 3

The EVCS considered for this paper has 30 outlets, each with 50 kW of power, i.e., a total load of 1500 kW. When EVCS is added to the RDN, the APL of the system increases, and the voltage profile decreases. It is crucial to disperse the EVCS as efficiently as possible to reduce the potential increase in APL. By connecting the fixed-capacity EVCS1 with a 1500 kW rating on bus 2, the APL obtained is 216.7893 kW. Additional EVCS installations are necessary to ensure that more EV users can use the EVCS. Thus, EVCS2, located on bus 19, with a 1500 kW rating, is also considered. It is observed that after connecting EVCS2 with bus 19, the APL for the bus increases to 227.9568 kW. The voltage profile after adding EVCS1 and EVCS2 is illustrated in Fig. 3, where the lowest magnitude is found on bus 18 with a voltage of 0.9116 p.u. and 0.9107 p.u., respectively. It may be noted that EVCSs and capacitors are not anticipated to be connected to bus 1, as it is a slack bus with a constant voltage of 1 p.u..

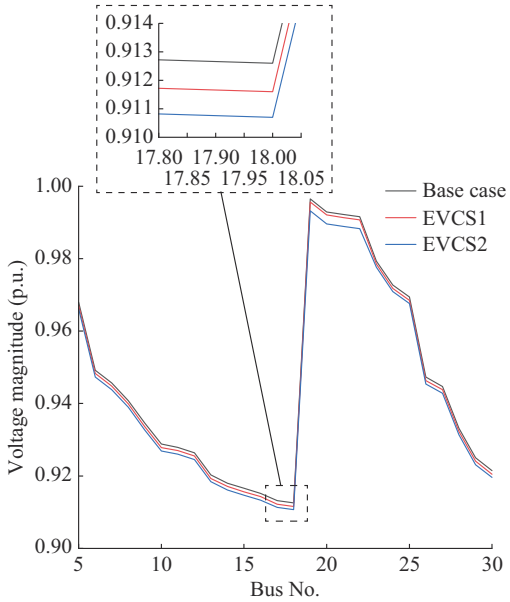

Fig. 3. Base case voltage profile of IEEE 33-bus RDN.

C. Scenario 4

To enhance the voltage profile and reduce loss, capacitors are positioned closer to the EVCS and at the ends of feeders. Here, a switched-type capacitor with RP injection set between the minimum and maximum values (150-1200 kvar) is utilized for compensation. The optimization model is solved through simulation on an Intel i9 64-bit PC running MATLAB-R2022b equipped with a 3.20 GHz CPU and 32 GB of RAM (12th Gen). The capacitor configuration results in decreased APL and improved voltage profiles. The primary objective of this paper is to reduce the APL due to resistive losses in the RDN.

Various scenarios considering different numbers of capacitors (1C-6C) are simulated for the IEEE 33-bus RDN utilizing the objective function given in (19). Optimal bus location and sizes in kvar of these capacitors in the presence of EVCS are obtained as shown in Table III, using different optimization algorithms such as GWO, PSO, CS, HPSO_CS, and HGWO_PSO. Table III shows that the APL decreases for the proposed optimization algorithms as the number of capacitors grows.

TABLE III
COMPARISON OF LOCATION, SIZE, AND APL WITH A CAPACITOR INSTALLATION IN IEEE 33-BUS RDN FOR ALL ALGORITHMS

Number of capacitors	PSO				CS				GWO				HGWO_PSO				HPSO_CS			
	Location	Size (kvar)	Total (kvar)	APL (kW)	Location	Size (kvar)	Total (kvar)	APL (kW)	Location	Size (kvar)	Total (kvar)	APL (kW)	Location	Size (kvar)	Total (kvar)	APL (kW)	Location	Size (kvar)	Total (kvar)	APL (kW)
1C	30	656	656	158.867	31	878	878	153.978	8	1058	1058	165.53	29	859	859	153.00	32	1102	1102	154.36
2C	12, 27	531, 815	1346	152.757	31, 23	952, 312	1264	149.603	8, 26	707, 374	1081	161.90	6, 29	793, 468	1261	149.02	33, 15	665, 491	1156	147.59
3C	5, 14, 29	616, 808, 471	1895	143.269	23, 27, 33	952, 368, 729	2049	143.458	6, 20, 26	342, 523, 931	1796	159.97	30, 23, 10	423, 719, 672	1814	145.22	30, 9, 8	778, 578, 535	1891	140.45
4C	14, 21, 25, 30	182, 270, 756, 987	2195	138.374	12, 22, 23, 30	158, 307, 615, 1027	2107	137.620	8, 20, 23, 26	250, 520, 380, 1090	2240	155.85	10, 22, 24, 29	350, 220, 510, 1017	2097	137.69	12, 20, 24, 30	320, 350, 570, 850	2090	136.52
5C	10, 25, 29, 31, 14	828, 493, 306, 689, 150	2466	144.241	24, 12, 19, 18, 29	367, 297, 612, 433, 613	2322	145.944	24, 4, 28, 22, 13	378, 597, 215, 424, 815	2429	160.65	23, 5, 18, 24, 29	286, 615, 458, 782, 325	2466	148.64	30, 22, 10, 17, 3	789, 167, 767, 229, 620	2568	143.76
6C	30, 14, 25, 33, 8, 31	365, 704, 428, 300, 727, 150	2674	150.648	22, 18, 31, 11, 24, 29	507, 418, 256, 233, 813, 387	2614	151.920	13, 8, 23, 4, 29,10	330, 1028, 732, 152, 570, 468	3280	164.56	20, 26, 5, 30, 17, 24	456, 374, 499, 248, 622, 279	2478	152.51	20, 4, 33, 12, 30, 26	263, 686, 451, 655, 510, 750	3315	150.90

Additionally, only 4C provides the least PL among all the capacitors, making it the right number to be allocated in the IEEE 33-bus RDN. As capacitors increase, they inject RP components [7] and reduce losses.

The convergence curve is plotted to check the performance of the proposed optimization algorithms. The convergence curve of various optimization algorithms for APL with simultaneous installation of EVCSs and capacitors in an IEEE 33-bus RDN over 1000 iterations is presented in Fig. 4.

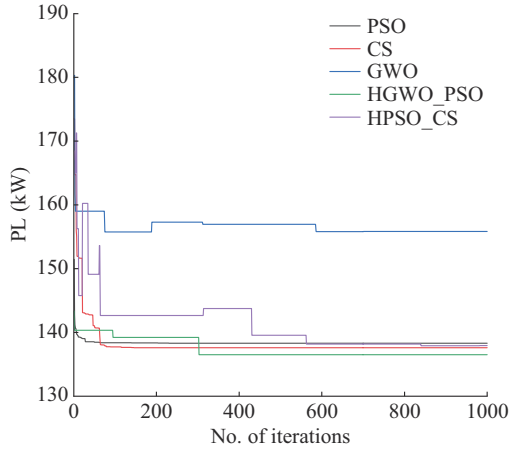

Fig. 4. Convergence curve of various optimization algorithms for APL with simutaneous installation of EVCSs and capacitors in IEEE 33-bus RDN.

Accordingly, it is observed that the proposed optimization algorithms produce quick convergence as compared with individual optimization algorithm. The total convergence time for various optimization algorithms with multiple installations of capacitors is given in Table IV. It is observed that if there is more PL, the optimization process becomes slower, leading to longer convergence time. The proposed optimization algorithms take more time to work with reduced power. If there is less PL, the optimization process becomes faster and more efficient, reducing the time needed to reach the optimal solution. The proposed optimization algorithms have given a quicker convergence speed than all other optimization algorithms.

However, once the right size and number of capacitors exceed the optimal values, i.e., 4C, there will be back-feeding of the RP injected by the capacitor, thereby increasing the system APL. The APL of the base case, with EVCS1 and EVCS2 along with capacitors, is shown in Fig. 5.

Figure 5 shows that APL increases from a base case of 204.7920 kW to 227.9568 kW with the addition of EVCS1 and EVCS2. Additionally, after adding capacitors, APL decreases subsequently, obtaining optimal PL at 4C, and then increases the PL as the number of capacitors increases to 5C and 6C. Additionally, from Table III, among GWO, PSO, CS, and hybrid algorithms, HPSO_CS and HGWO_PSO result in the largest APL reduction, i.e., 137.69 kW and 136.52 kW, respectively, which leads to lower expenses associated with energy losses. Table V highlights the energy loss cost and percentage of energy loss cost reduction of the base case compared with the proposed optimization algorithms. As hybrid algorithms, HPSO_CS and HGWO_PSO provide superior loss reduction, i.e., 33.34% and 32.77%, respectively. Adding the capacitor configuration to the IEEE 33-bus RDN in the presence of EVCS decreases the APL and improves the voltage profile.. The comparisons of benefit of loss reduction curve for all optimization algorithms are shown in Fig. 6.

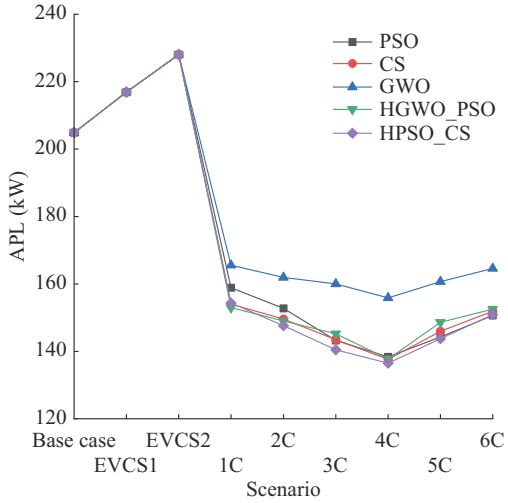

Fig. 5. Effect of EVCSs with capacitors on an APL curve for various algorithms.

TABLE IV
TOTAL CONVERGENCE TIME FOR VARIOUS OPTIMIZATION ALGORITHMS

Number of capacitors	Total convergence time (s)				
	PSO	Cuckoo	GWO	HGWO_PSO	HPSO_CS
1C	488.458	294.113	1206.499	459.344	162.375
2C	477.575	266.573	1123.650	444.712	153.286
3C	457.989	253.296	1059.330	420.779	147.746
4C	428.432	244.105	968.702	417.199	143.684
5C	446.101	250.761	1136.650	419.411	149.661
6C	480.763	288.130	1232.730	421.398	154.431

TABLE V
COMPARISONS OF ENERGY LOSS REDUCTION FOR VARIOUS OPTIMIZATION ALGORITHMS

Optimization algorithm	Energy loss cost ($)	Energy loss cost reduction (%)
Base case	107638.70	-
PSO	72729.22	32.43
CS	72333.18	32.80
GWO	81913.13	23.90
HGWO_PSO	72370.28	32.77
HPSO_CS	71755.91	33.34

Accordingly, the maximum benefit of loss reduction corresponding to optimal number and location of capacitor corresponds to 25729 $/year for GWO, 34911 $/year for PSO, 35306 $/year for CS, 35884 $/year for HPSO_CS, and 35268 $/year for HGWO_PSO.

Figure 7 depicts the benefit of EIC reduction for various optimization algorithms. As the number of capacitors increases, the benefit of EIC reduction increases until it reaches a peak at the optimal operation point. Adding more capacitors initially reduces EIC, but there is a point where further increases do not bring as much benefit. Beyond this point, the EIC reduction starts decreasing. Figure 7 also highlights that hybrid algorithms provide the maximum EIC benefit.

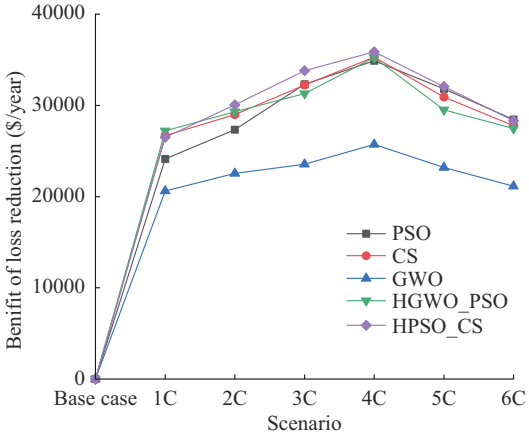

Fig. 6. Comparisons of benefit of loss reduction curve for various optimization algorithms.

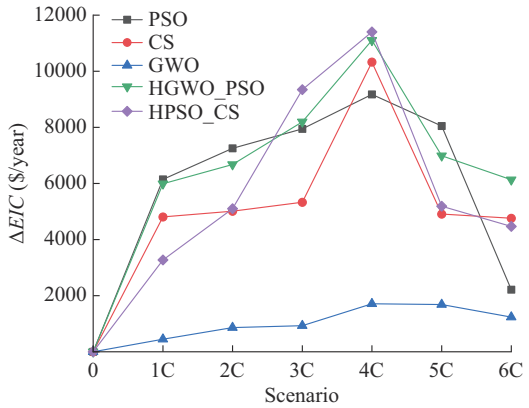

Fig. 7. Benefit of EIC reduction curve for various optimization algorithms.

Table V illustrates the proposed optimization algorithms, produces significant EIC reduction ranging from 2.60% to 16.45% compared with a baseline EIC of 374127.8 $/year at the optimal operation point. Furthermore, Table VI shows that the proposed optimization algorithms have the highest yearly benefit from EIC reduction. The size and IC of a capacitor are positively correlated. As a result, when capacitor size increases, the cost of producing or purchasing the capacitor rises linearly, as depicted in Fig. 8.

TABLE VI
COMPARISONS OF EIC REDUCTION AND ΔEIC FOR ALL OPTIMIZATION ALGORITHMS

Optimization algorithm	EIC ($)	EIC reduction (%)	ΔEIC ($)
Base case	374127.8	-	-
PSO	321860.3	13.97	9178.173
CS	315347.1	15.71	10321.890
GWO	364387.6	2.60	1710.379
HGWO_PSO	314613.5	15.90	11105.690
HPSO_CS	312597.9	16.45	11404.650

The main goal is to obtain the highest annual NPV, as described in (19). The maximum NPV (MNPV) amount with varying capacitors for various optimization algorithms is shown in Fig. 9.

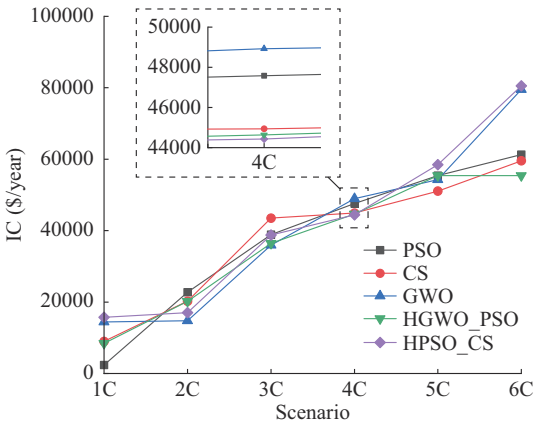

Fig. 8. IC of capacitor for various optimization algorithms.

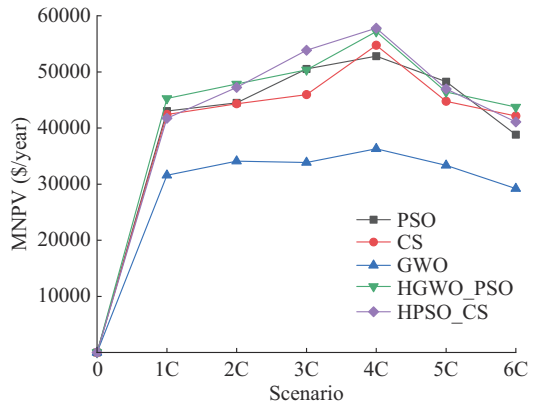

Fig. 9. MNPV for various optimization algorithms.

As the number of capacitors increases, NPV increases to the maximum value, i. e., MNPV. The highest annual NPV represented as the MNPV curve for GWO, PSO, CS, HPSO_CS, and HGWO_PSO is found to be 36282, 52813, 54750, 57786, and 57177 $/year, respectively. HPSO_CS produces a higher NPV when compared with all other optimization algorithms.

D. Scenario 5

In V2G mode, EVs can feed extra energy into the grid to support system stability. In the given EVCS for an optimal number of capacitors and sizes in the IEEE 33-bus RDN, the impact of the V2G mode of EVs is also studied. The improvement in voltage profile for all the IEEE 33-bus RDN for the base case, EVCS integration, and various penetration levels of V2G mode ranging from 5% to 30% with a step of 5% is presented, as shown in Fig. 10. It is observed that the voltage profile is improved upon EV participation in V2G mode. Furthermore, Fig. 10 clearly shows that as the percentage of EVs in V2G mode increases, there is a noticeable improvement in the voltage profile. Thus, the V2G mode benefits grid operators by maintaining an improved stable voltage profile in the RDN.

For the optimal EVCS nodes on buses 2 and 19 in the RDN, the APL is computed for various penetration levels of V2G mode from 5% to 30%. Figure 11 shows the APL reduction in IEEE 33-bus RDN with increased EV penetration level in V2G mode, compared with the base case for buses 2 and 19.

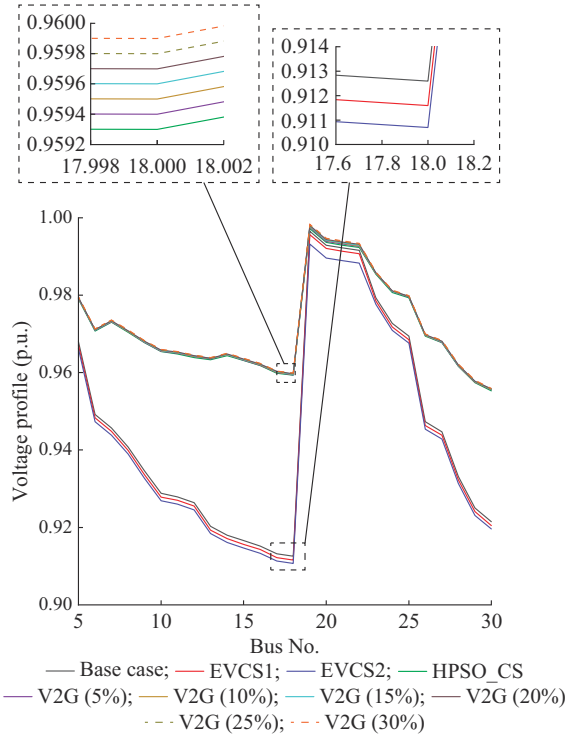

Fig. 10. Improvement in voltage profile in V2G mode.

Thus, the viability of V2G mode in the EVCS enables the PL reduction in the network. Figure 12 compares the APL reduction in IEEE 33-bus RDN for PSO, GWO, CS, HGWO_PSO, and HPSO_CS for the base case in the presence of EVCS and variation in penetration level of V2G mode. Here, the APL reduction is observed with the increase in the penetration level of V2G mode. Additionally, it is observed that HPSO_CS provides the lowest APL. The APL is found to be 135.2851, 134.5936, 133.94, 133.3242, 132.9347, and 132.2061 kW, with penetration levels of 5%, 10%, 15%, 20%, 25%, and 30%, respectively.

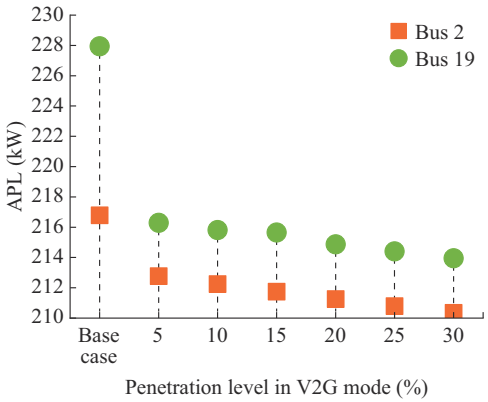

Fig. 11. APL reduction for IEEE 33-bus RDN with increased EV penetration level in V2G mode.

Considering the economic benefit of the V2G mode of operation, the APL reduction increases the revenue of the network operator. To illustrate this point, Fig. 13 shows the increased MNPV as the penetration level increases.

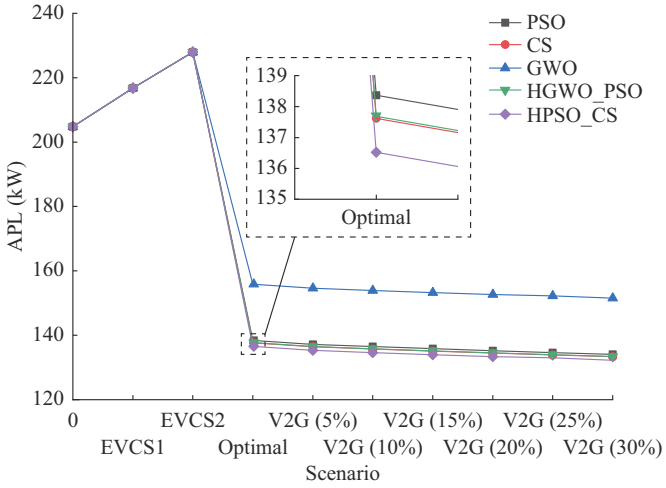

Fig. 12. Comparisons of APL reduction for various optimization algorithms in V2G mode.

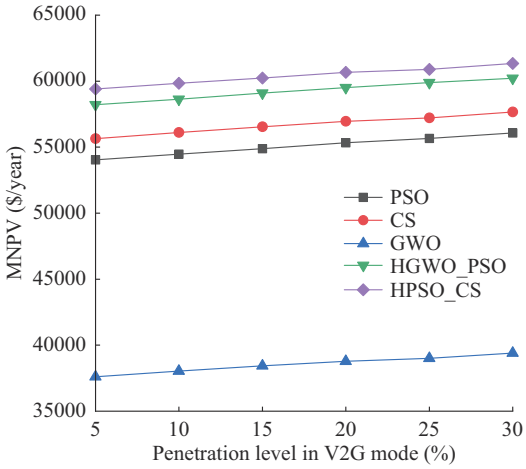

Fig. 13. MNPV for various optimization algorithms in V2G mode.

Additionally, Fig. 13 highlights that HPSO_CS indicates the highest MNPV values for the V2G mode of operation, thereby providing the best results.

V. Conclusion

In this paper, economically driven optimal simultaneous allocation of EVCSs and capacitors in RDN is studied by considering the benefit of energy loss reduction and EIC along with the cost of EVCSs and capacitors. The proposed optimizaiton algorithms are validated in the IEEE 33-bus RDN. It is noticed that when EVCS is added to the RDN, the APL of the system increases, and the voltage profile decreases. It is observed that the proposed HGWO_PSO and HPSO_CS allow us to determine the appropriate location of capacitors and sizes. In the IEEE 33-bus RDN with EVCS, adding the capacitor configuration reduces the APL and EIC cost and enhances the voltage profile. Additionally, HPSO_CS converges quickly and achieves a higher profit when compared with individual optimization algorithms. Furthermore, for V2G mode, the proposed optimization algorithms with the given objective function present superior performance, thereby allowing the operator to plan and conduct a cost-benefit analysis properly.

References

[1] IEA. (2022, May). Global EV outlook 2022 analysis IEA. [Online]. Available: https://www.iea.org/reports/global-ev-outlook-2022

[2] Department of Heavy Industry. (2017, Mar.). National electric mobility mission plan. [Online]. Available: http://dhi.nic.in

[3] M. Etezadi-Amoli, K. Choma, and J. Stefani, "Rapid-charge electric-vehicle stations," *IEEE Transactions on Power Delivery*, vol. 25, no. 3, pp. 1883-1887, Jul. 2010.

[4] H. Mehrjerdi and E. Rakhshani, "Vehicle-to-grid technology for cost reduction and uncertainty management integrated with solar power," *Journal of Cleaner Production*, vol. 229, pp. 463-469, Aug. 2019.

[5] G. Lin, J. Liu, R. Christian *et al*., "Inertia droop control and stability mechanism analysis of energy storage systems for dc-busbar electric vehicle charging station," *IEEE Transactions on Transportation Electrification*, vol. 9, no. 1, pp. 266-282, Mar. 2023.

[6] M. E. Baran and F. Wu, "Network reconfiguration in distribution systems for loss reduction and load balancing," *IEEE Transactions on Power Delivery*, vol. 4, no. 2, pp. 1401-1407, Apr. 1989.

[7] Y. Xu, Z. Y. Dong, K. P. Wong *et al*., "Optimal capacitor placement to distribution transformers for power loss reduction in radial distribution systems," *IEEE Transactions on Power Systems*, vol. 28, no. 4, pp. 4072-4079, Nov. 2013.

[8] R. F. Cook, "Optimizing the application of shunt capacitors for reactive-volt-ampere control and loss reduction," *Transactions of the American Institute of Electrical Engineers, Part III: Power Apparatus and Systems*, vol. 80, no. 3, pp. 430-441, Apr. 1961.

[9] R. N. Allan, R. Billinton, I. Sjarief *et al*., "A reliability test system for educational purposes: basic distribution system data and results," *IEEE Transactions on Power Systems*, vol. 6, no. 2, pp. 813-820, Feb. 1991.

[10] K. Prakash and M. Sydulu, "Particle swarm optimization based capacitor placement on radial distribution systems," in *Proceedings of 2007 IEEE PES General Meeting*, Tampa, USA, Jul. 2007, pp. 1-5.

[11] Z. Liu, F. Wen, and G. Ledwich, "Optimal planning of electric-vehicle charging stations in distribution systems," *IEEE Transactions on Power Delivery*, vol. 28, no. 1, pp. 102-110, Jan. 2013

[12] T. Chen, X. P. Zhang, J. Wang *et al*., "A review on electric vehicle charging infrastructure development in the UK," *Journal of Modern Power Systems and Clean Energy*, vol. 8, no. 2, pp. 193-205, Mar. 2020.

[13] J. Shen, C. Jiang, and B. Li, "Controllable load management approaches in smart grids," *Energies*, vol. 8, no. 10, pp. 11187-11202, Oct. 2015.

[14] R. Arulraj and N. Kumarappan, "Optimal economic-driven planning of multiple DG and capacitor in distribution network considering different compensation coefficients in feeder's failure rate evaluation," *Engineering Science and Technology, an International Journal*, vol. 22, no. 1, pp. 67-77, Feb. 2019.

[15] B. Canizes, J. Soares, Z. Vale *et al*., "Optimal approach for reliability assessment in radial distribution networks," *IEEE Systems Journal*, vol. 11, no. 3, pp. 1846-1856, Sept. 2017.

[16] P. Rajesh and F. H. Shajin, "Optimal allocation of EV charging spots and capacitors in distribution network improving voltage and power loss by quantum-behaved and Gaussian mutational dragonfly algorithm (QGDA)," *Electric Power Systems Research*, vol. 194, p. 107049, May 2021.

[17] M. Bilala and M. Rizwan, "Integration of electric vehicle charging stations and capacitors in distribution systems with the vehicle-to-grid facility," *Energy Sources*, vol. 8, pp. 1-30, Apr. 2021.

[18] M. Bilal, M. Rizwan, I. Alsaidan *et al*., "AI-based approach for optimal placement of EVCS and DG with reliability analysis," *IEEE Access*, vol. 9, pp. 154204-154224, Nov. 2021.

[19] B. Leonardo, T. P. Abud, B. H. Dias, "Optimal location of EV charging stations in a neighborhood considering a multi-objective approach," *Electric Power Systems Research*, vol. 199, p. 107391, Oct. 2021.

[20] S. Gupta, V. K. Yadav, and M. Singh, "Optimal allocation of capacitors in radial distribution networks using Shannon's entropy," *IEEE Transactions on Power Delivery*, vol. 37, no. 3, pp. 2245-2255, Jun. 2022.

[21] L. A. Gallego, J. M. Lopez-Lezama, and O. G. Carmona, "A mixed-integer linear programming model for simultaneous optimal reconfigura-

tion and optimal placement of capacitor banks in distribution networks," *IEEE Access*, vol. 10, pp. 52655-52673, May 2022.
[22] B. T. Geetha, A. Prakash, S. Jeyasudha *et al*., "Hybrid approach based combined allocation of electric vehicle charging stations and capacitors in distribution systems," *Journal of Energy Storage*, vol. 72, p. 108273, Nov. 2023.
[23] B. V. Kumar and A. F. M A, "A review of technical impact of electrical vehicle charging stations on distribution grid," in *Proceedings of 2023 International Conference on Recent Advances in Electrical, Electronics & Digital Healthcare Technologies (REEDCON)*, New Delhi, India, pp. 559-564, May 2023.
[24] P. Roy, R. Ilka, J. He *et al*., "Impact of electric vehicle charging on power distribution systems: a case study of the grid in western Kentucky," *IEEE Access*, vol. 11, pp. 49002-49023, May 2023.
[25] A. G. Trojani, J. M. Baigi, and M. S. Moghaddam, "Stochastic security-constrained unit commitment considering electric vehicles, energy storage systems, and flexible loads with renewable energy resources," *Journal of Modern Power Systems and Clean Energy*, vol. 11, no. 5, pp. 1405-1414, Sept. 2023.
[26] N. Pompern, S. Premrudeepreechacharn, A. Siritaratiwat *et al*., "Optimal placement and capacity of battery energy storage system in distribution networks integrated with PV and EVs using metaheuristic algorithms," *IEEE Access*, vol. 11, pp. 68379-68394, Jul. 2023.
[27] H. Wang, M. Shi, P. Xie *et al*., "Electric vehicle charging scheduling strategy for supporting load flattening under uncertain electric vehicle departures," *Journal of Modern Power Systems and Clean Energy*, vol. 11, no. 5, pp. 1634-1645, Sept. 2023.
[28] W. Dai, C. Wang, H. H. Goh *et al*., "Hosting capacity evaluation method for power distribution networks integrated with electric vehicles," *Journal of Modern Power Systems and Clean Energy*, vol. 11, no. 5, pp. 1564-1575, Sept. 2023.
[29] A. A. A. El-Ela, R. A. El-Sehiemy, A. M. Kinawy *et al*., "Optimal capacitor placement in distribution systems for power loss reduction and voltage profile improvement," *IET Generation, Transmission & Distribution*, vol. 10, no. 5, pp. 1117-1311, Apr. 2016.
[30] J. Jin, H. Li, R. Yang *et al*., "An improved compensation method for voltage sags and swells of the electric vehicles charging station based on a UPQC-SMES system," *Journal of Electrical Power & Energy Systems*, vol. 143, p. 108501, Dec. 2022.
[31] A. H. Etemadi and M. F. Firuzabad, "Distribution system reliability enhancement using optimal capacitor placement," *IET Generation, Transmission & Distribution*, vol. 2, no. 5, pp. 621-631, Sept. 2008.
[32] Delhi Electricity Regulatory Commission. (2003, Jun.). Complaint handling procedure relating to distribution and retail supply. [Online]. Available: https://www. derc. gov. in/consumers-corner/complaint-handling-procedures
[33] L. Goel and R. Billinton, "Evaluation of interrupted energy assessment rates in distribution systems," *IEEE Transactions on Power Delivery*, vol. 6, no. 4, pp. 1876-1882, Oct. 1991.
[34] E. N. Dialynas, S. M. Megaloconomos, and V. C. Dali, "Interruption cost analysis for the electrical power customers in Greece," in *Proceedings of 16th International Conference and Exhibition on Electricity Distribution*, Amsterdam, Netherlands, Jun. 2001, pp. 1-8.
[35] H. Patil and V. N. Kalkhambkar, "Grid integration of electric vehicles for economic benefits: a review," *Journal of Modern Power Systems and Clean Energy*, vol. 9, no. 1, pp. 13-26, Jan. 2021.
[36] K. E. Adetunji, I. W. Hofsajer, A. M. Abu-Mahfouz *et al*., "A review of metaheuristic techniques for optimal integration of electrical units in distribution networks," *IEEE Access*, vol. 9, pp. 5046-5068, Sept. 2021.
[37] J. Ding, Q. Wang, Q. Zhang *et al*., "A hybrid particle swarm optimization-cuckoo search algorithm and its engineering applications," *Hindawi Mathematical Problems in Engineering*, vol. 2019, pp. 1-12, Mar. 2019.
[38] M. A. M. Shaheen, H. M. Hasanien, and A. Alkuhayli, "A novel hybrid GWO-PSO optimization technique for optimal reactive power dispatch problem solution," *Ain Shams Engineering Journal*, vol. 12, no. 1, pp. 621-630, Mar. 2021.
[39] V. Vita, "Development of a decision-making algorithm for the optimum size and placement of distributed generation units in distribution networks," *Energies*, vol. 10, no. 9, p. 1433, Sept. 2017.

B. Vinod Kumar received the B.Tech. degree in electrical and electronic engineering from Guru Nanak Engineering College (Now Guru Nanak University), Hyderabad, India, in 2012, and the M.Tech. degree in high voltage engineering, which is a part of electrical engineering from National Institute of Technology Calicut, Kozhikode, India, in 2019. He is pursuing the Ph.D. degree in electrical and electronic engineering at the National Institute of Technology in Tiruchirappalli, Tiruchirappalli, India. His research interests include electric vehicle integration, electric vehicle impacts on distribution networks, power system reliability, and power system optimization.

Aneesa Farhan M A received the B.Tech. degree from M.E.S College of Engineering, Calicut University, Kozhikode, India, in 2006, the M.E. degree in electrical engineering from the Indian Institute of Science Bangalore, Bangalore, India, in 2008, and the Ph.D. degree in electrical engineering from the Indian Institute of Technology Madras, Chennai, India, in 2019. She has worked as Assistant Engineer for 3 years at Kerala State Electricity Board, India. Currently, she is with the National Institute of Technology Tiruchirappalli, Tiruchirappalli, India, working as an Assistant Professor in the Department of Electrical and Electronics Engineering since May 2020. Her research interests include distributed generation, microgrid, microgrid protection, energy management in microgrids, electric vehicle integration into grid, and power system optimization.